Materials and Design 187 (2020) 108392

Contents lists available at ScienceDirect

Materials and Design

journal homepage: www.elsevier.com/locate/matdes

Predicting the stacking fault energy of austenitic Fe-Mn-Al (Si) alloys

Young Won Choi [a,*], Zhihua Dong [a], Wei Li [a], Stephan Schönecker [a], Hansoo Kim [b], Se Kyun Kwon [c,*], Levente Vitos [a,d,e,**]

[a] Applied Materials Physics, Department of Materials Science and Engineering, Royal Institute of Technology, SE-100 44 Stockholm, Sweden
[b] Institute of High Technology Materials and Devices, Korea University, Seoul 02841, Republic of Korea
[c] Department of Physics, Pohang University of Science and Technology, Pohang 37673, Republic of Korea
[d] Department of Physics and Astronomy, Division of Materials Theory, Uppsala University, Box 516, SE-75121 Uppsala, Sweden
[e] Research Institute for Solid State Physics and Optics, Wigner Research Center for Physics, P.O. Box 49, H-1525 Budapest, Hungary

HIGHLIGHTS

- Traditional floating spin models fail to account for the experimental trends.
- Longitudinal spin fluctuations yield stacking fault energies in good agreement with experiments.
- The magnetic state of the host Fe-Mn alloy is determinative for the alloying trends on the stacking fault energy.

GRAPHICAL ABSTRACT

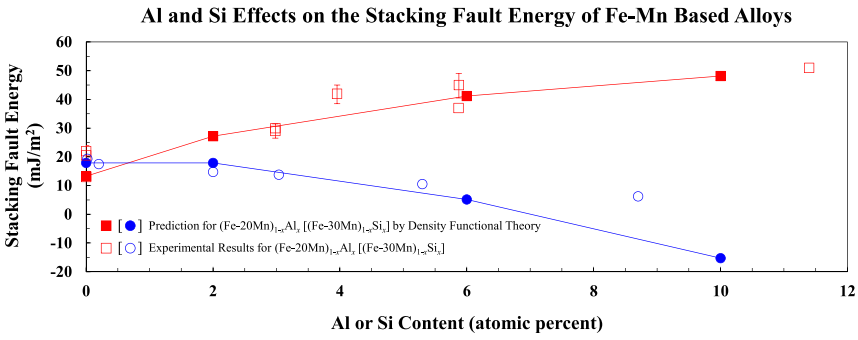

ARTICLE INFO

Article history:
Received 18 October 2019
Received in revised form 27 November 2019
Accepted 28 November 2019
Available online 29 November 2019

Keywords:
Stacking-fault energy
Austenitic steel
First-principles calculation
Magnetism
Longitudinal spin fluctuation

ABSTRACT

Aluminum and silicon are common alloying elements for tuning the stacking fault energy (SFE) of high Mn steels. Today the theoretical investigations on the Fe-Mn-Al/Si systems using Density Functional Theory (DFT) are very scarce. In the present study, we employ a state-of-the-art longitudinal spin fluctuations (LSFs) model in combination with DFT for describing the magnetic effects in Fe-Mn based alloys at finite temperature. We find that the traditional DFT-floating spin results fail to explain the experimental trends. However, the DFT-LSFs approach properly captures the Al-induced increase and Si-induced decrease of the SFE of the base alloy in line with the room-temperature observations. This finding highlights the importance of LSFs in describing the Al/Si effects on the SFE of Fe-Mn based alloys. We point out that the effects of the non-magnetic Al and Si additions on the SFE are in fact determined by the magnetic state of the host matrix. In addition, we estimate the role of carbon addition in the alloying effects of Al and Si. The present results provide a convenient pathway to access the important mechanical parameters for designing advanced high-strength alloys.

* Corresponding authors.
** Correspondence to: L. Vitos, Applied Materials Physics, Department of Materials Science and Engineering, Royal Institute of Technology, SE-100 44 Stockholm, Sweden.
E-mail addresses: ywchoi@kth.se (Y.W. Choi), sekk@postech.ac.kr (S.K. Kwon), levente@kth.se (L. Vitos).

https://doi.org/10.1016/j.matdes.2019.108392

1. Introduction

High Mn steels have been considered as prominent candidates for automobile structural components due to their excellent mechanical properties [1–11]. The mechanical performance of high Mn steels depends on the plastic deformation mechanisms such as transformation-induced plasticity (TRIP), twinning-induced plasticity (TWIP), and dislocation glide [12–14]. It is well recognized that the stacking fault energy (SFE) is a key physical quantity, which governs the active deformation mechanism [12,15–18]. Therefore, it is of crucial importance to understand the dependence of the SFE on the chemical composition with an appropriate description method [19–24].

It is experimentally observed that Al increases [25–32] the SFE of austenitic Fe-Mn alloys whereas Si decreases it [28,33]. Thanks to the developments of computational methodology during the last decade, today the SFE of steel alloys and other complex multi-component systems can routinely be accessed by using *ab initio* methods [34–39]. In addition to the systematic data production, such an atomistic modeling allows us to look deep inside the problem and identify the key mechanism responsible for the observed material properties. However, despite the large number of theoretical reports on this subject, so far *ab initio* studies on the effects of Al and Si regarding the SFE of Fe-Mn alloys are very scarce. This may partly be because of the difficulty of properly describing the SFE of Fe-Mn based alloys. To obtain the SFE with high precision is indeed a big challenge due to its complex thermo-magneto-chemical behavior [40]. Here, we make use of the most recent advances in theoretical modeling of high-temperature magnetism to approach the questions.

To the best of our knowledge, there is a single density functional theory (DFT) investigation which predicted correctly the increase of the SFE by Al [41]. However, those results imply that the hexagonal close-packed (hcp) phase is more stable than the face-centered cubic (fcc) phase, which is contradictory because the system exists in fcc phase at ambient conditions. Furthermore, the previous work did not consider finite temperature effects on the SFE and thus could not study the alloying effects at room temperature.

It is usually accepted that the magnetic structure of austenitic Fe-Mn alloys is antiferromagnetic at room temperature for Mn content more than 15 wt% [42]. However, the experimental specimens usually contain a certain level of carbon, which affects the Néel temperature (T_N). From the experimental data, the magnetic transition temperature depends on compositions as $T_N = 250 \ln(x_{Mn}) - 4750 x_C x_{Mn} + 720$ (K), where x_C and x_{Mn} are the mole fractions of C and Mn, respectively [43]. According to this empirical expression, T_N for Fe-18Mn-0.6C (wt%), which is a typical composition of high manganese steel, is 267 K. Therefore, one should adopt a paramagnetic state for describing the magnetism in Fe-Mn as far as one is to model the experimental specimen at room temperature and above.

One effective way to simulate the paramagnetic state is to employ the disordered local magnetic moment (DLM) picture [44,45], where the local magnetic moments are sustained even above the magnetic ordering temperature, but the total magnetization vanishes. Traditionally, this problem has been treated by the floating spin (FS) calculations, where the magnitude of the local moments is computed self-consistently from the Kohn-Sham equations. Here we go beyond this static scheme and consider the longitudinal spin fluctuations (LSFs). Previous studies show that the LSFs are crucial for describing the SFE of Fe-Mn alloys at finite temperature [40]. We extend the computational scheme and apply it to the Fe-Mn-Al (Si) ternary alloys.

The present paper is organized as follows. First we examine the bulk properties of Fe-Mn alloys as a preliminary study, and examine the effects of Al and Si addition on these properties. Next, we explore alloying effects on the SFE of Fe-Mn alloys using both of the FS and LSFs schemes. The results are compared with the experimental results. From the FS and LSFs data, we establish the key mechanism responsible for the observed alloying effects. Finally, by considering the volume-induced effects of interstitials, we estimate and discuss the impact of small amount of carbon addition on the above alloying trends of the SFE.

2. Methods

The total energy calculations were performed using DFT [46,47] as implemented on the Exact Muffin-tin Orbitals (EMTO) method [48]. The local-density approximation (LDA) [47] was used in self-consistent calculations, and the generalized-gradient approximation (GGA) [49] as parametrized by Perdew-Burke-Ernzerhof (PBE) [50] was adopted for the total energy. We described the paramagnetic state within the DLM model [44,45] in combination with the coherent potential approximation (CPA) [51,52]. The chemical disorder was treated also with the CPA. We considered Al and Si up to 10 atomic percent (at.%) added to Fe-20Mn and Fe-30Mn (at.%) alloys, respectively, keeping the ratio of Fe and Mn constant. In this way we can systematically test the interatomic interaction among the alloying elements in the materials.

The SFE was evaluated by constructing a supercell structure. A stacking fault was incorporated in the 6 layered supercell along the [111] direction of the fcc structure. Our previous studies show that 6 layers are enough to guarantee the convergence of the SFE with respect to the number of layers in the supercell [40]. In order to access the SFE at finite temperature, we adopted the Helmholtz free energy. The Helmholtz free energy F consists of the internal energy E and the –TS term, where T is the temperature and S the entropy. Here, the entropy can be divided into electronic, vibrational, and magnetic contributions. According to our tests, the electronic entropy is insignificant at room temperature and thus it is omitted from the beginning. The SFE is defined as $\gamma = \frac{F_{sf} - F_{perfect}}{A}$, where F_{sf} and $F_{perfect}$ are the free energies of the structure with faults and perfect fcc structure, respectively, and A is the unit area. Then, γ can be decomposed into the internal energy contribution, $\gamma_{int} \equiv \frac{E_{sf} - E_{perfect}}{A}$ and the vibrational and magnetic contribution, $\gamma_{vib} \equiv \frac{(-TS_{vib,sf}) - (-TS_{vib,perfect})}{A}$ and $\gamma_{mag} \equiv \frac{(-TS_{mag,sf}) - (-TS_{mag,perfect})}{A}$, respectively. The effect of phonons on the SFE, γ_{vib}, was estimated to be small, about 2 mJ/m^2 for fcc Fe, at the temperature region considered here [38], which can safely be omitted in the following discussions. We obtained the internal energies from standard total energy calculations and the magnetic entropy from the mean-field approximation, $S_{mag} = k_B \sum_{\{I,i\}} c_{I,i} \ln(1 + m_{I,i})$, where k_B is the Boltzmann constant, $c_{I,i}$ is the concentration of species i at site I, and $m_{I,i}$ is the corresponding local magnetic moment. The possibility of segregation near the stacking fault was not considered and thus the configurational entropy contribution to the SFE vanishes.

The LSFs effects on the magnetic moment in the bulk and the free energy were considered as follows. First we obtained the static equilibrium magnetic moment (μ_0) through conventional spin-polarized DFT calculations based on the CPA and DLM model, so called FS calculations. In these calculations, we may use the primitive cell of the fcc structure. Next, we derived the energy distribution $E_i(\mu)$ depending on the magnitude of the magnetic moment μ for each component i using spin-constraint calculations. Except the target component, we fixed the magnetic moments of the others to the static equilibrium values. Then, from the LSFs energy for each alloying component $E_{LSFs,i}(\mu) = \{E_i(\mu) - E_i(0)\}/c_i$, we computed the probability distribution $x_i(\mu) = \mu^2 \exp(-E_{LSFs,i}(\mu)/k_BT)/Z$ at temperature T with the partition function $Z = \int_0^\infty \mu^2 \exp(-E_{LSFs,i}(\mu)/k_BT) d\mu$. Note that the fluctuating medium approximation (FMA) [53] was drawn upon here for obtaining the LSFs energy. We finally get the root mean square value of the magnetic moment $m_i = \sqrt{\int_0^\infty \mu^2 x_i(\mu) d\mu}$. We used this magnetic moment value to quantify

the LSFs effect. The detailed theoretical background for the LSFs can be found in Refs. [53–55].

In the case for the fcc Fe-Mn-Al (Si) alloys, we took $E_i(\mu)$ in the range of 0 to 3.0 μ_B with the interval of 0.5 μ_B for Fe and Mn, and in the range of 0 to 0.5 μ_B with the interval of 0.1 μ_B for Al (Si). For the supercell involving the stacking fault, the procedure to obtain the mean magnetic moments is as follows. First we found the moment of each alloying element in the sequence of Al (Si), Mn, and Fe for the 1st nearest-neighbor (nn) sites to the stacking fault plane by fixing the moments of the other sites to the bulk values $m_{\text{bulk},\,i}$. Then we went on to the next-nearest neighbors with the 1st nearest-neighbor moments $m_{1\text{ nn},\,i}$. When we considered $E_i(\mu)$ for Al (Si), we adopted the magnetic moments of Mn and Fe in the same layer from the FS calculations. The obtained moment for Al (Si) was successively used as a background to calculate $E_i(\mu)$ for Mn. In the same way, for Fe, the Al (Si) and Mn moments are used as a background.

In principle, all m_i's should be self-consistently determined through iterative calculations. This procedure is very time-consuming and would not influence the final moments significantly when the magnetic interaction among alloying components is weak, for example, above the magnetic transition temperature. Therefore, we skipped the cumbersome iteration procedure and performed the one-shot calculation from static equilibrium approach [53].

All the calculations were performed for $T = 298$ K. Since the results are strongly volume dependent, in order to avoid any inconsistency between theory and experiment, we employed the experimental volumes in our calculations. For the volume of Fe-Mn alloys, we referred to the study by Li et al. [56], and for the effects of Al and Si on the volume of Fe-Mn alloys, we referred to Jung and De Cooman [65] and Lu et al. [58], respectively. All the experimental volumes were measured at room temperature, and therefore the finite temperature effects were also considered indirectly.

3. Results

Fig. 1 shows the static equilibrium magnetic moment (μ_0) and mean magnetic moment induced by spin fluctuation (m_i) for the bulk depending on the composition in Fe-Mn alloys. First we find that the mean magnetic moment is larger than the static magnetic moment by about 0.15 μ_B and 0.5 μ_B for Fe and Mn, respectively, regardless of the alloy composition. For example, the mean magnetic moments of Fe-0.5Mn (at.%) alloy are $m_{\text{Fe}} = 1.55\ \mu_B$ and $m_{\text{Mn}} = 1.39\ \mu_B$ for Fe and Mn, respectively, and the static moments of the same alloy are $\mu_{0,\,\text{Fe}} = 1.40\ \mu_B$ and $\mu_{0,\,\text{Mn}} = 0.88\ \mu_B$, which gives $\Delta\mu = m_i - \mu_{0,\,i} = 0.15\ \mu_B$ and 0.51 μ_B for i = Fe and Mn, respectively. It is also observed that all the magnetic moments weakly increase by increasing Mn content. When Mn content increases from 0.5 to 30 at.%, $\mu_{0,\,\text{Fe}}$ and $\mu_{0,\,\text{Mn}}$ increase only about 0.03 μ_B and 0.10 μ_B, which are negligible compared to the original values $\mu_{0,\,\text{Fe}} = 1.40\ \mu_B$ and $\mu_{0,\,\text{Mn}} = 0.88\ \mu_B$ of Fe-0.5Mn (at.%). The change of the mean magnetic moment by varying Mn content is also in a similar size. Hence, the difference between the static magnetic moment and the mean magnetic moment of Fe-Mn alloys remains almost a constant independent of alloy composition.

Fig. 2(a) and (b) show the effect of Al addition on the static equilibrium magnetic moment and the mean magnetic moment in Fe-20Mn (at.%) alloy, respectively. As the Al content increases, μ_0's of Fe and Mn increase as found in Fig. 2(a). The sizes of the static magnetic moment increment by 10 at.% Al addition are 0.15 μ_B and 0.45 μ_B for Fe and Mn, respectively. We can also find a similar trend of the mean magnetic moment in Fig. 2(b). However, in this case the changes are reduced by about a half of those of μ_0, $\Delta m_{\text{Fe}} = 0.09\ \mu_B$ and $\Delta m_{\text{Mn}} = 0.20\ \mu_B$ with 10 at.% Al addition. We note that the chemical effect of Al reduces the size of Fe magnetic moment in the considered composition range perhaps due to the weakening of the exchange coupling of Fe atom with its neighbors. However, in general Al causes a volume increment in austenitic Fe-Mn alloys. It is interesting that the volumetric effect by Al surmounts the chemical contribution and the main features of the magnetic moment by Al addition in Fe-20Mn (at.%) is reasonably well captured by the lattice expansion effect.

In Fig. 3, we show the Si alloying effect on the local magnetic moment of Fe-30Mn (at.%) alloys. Fig. 3(a) shows that the Si alloying decreases both the static magnetic moments of Fe and Mn in Fe-30Mn (at.%) alloys. As the Si concentration increases from 0 to 10 at.%, the static moments decrease by 0.14 μ_B and 0.06 μ_B for Fe and Mn, respectively. This fact can be understood by taking into account the volume contraction induced by Si addition. Meanwhile, the behavior of the mean magnetic moment is qualitatively similar to that of the static moment. It is also seen that, similarly to the case of Al addition, the Si alloying effects on the magnetic moments can be estimated mainly from the lattice variation, except μ_0 of Mn in which the chemical effect acts in the opposite direction and causes the net result to be almost null. Note that the effect of Si on the lattice parameter is weaker than that of Al, about one-third in magnitude. Hence, we observe only tiny changes of the local magnetic moments, especially for the mean moments in Fig. 3(b).

Here, it is clear that a proper account of magnetic degrees of freedom would be crucial for a further theoretical study of materials properties. With the two established descriptions of magnetic states, we go into

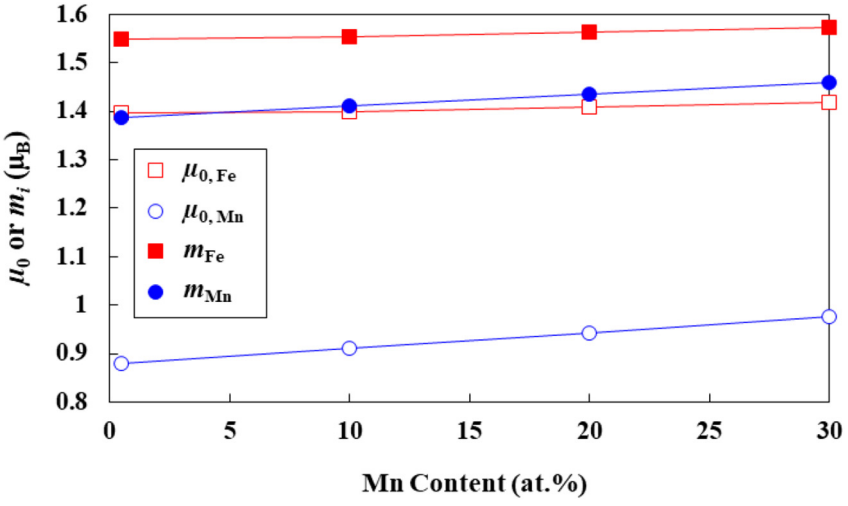

Fig. 1. Static equilibrium local magnetic moment (μ_0) and mean magnetic moment induced by the LSFs (m_i) in the bulk of Fe-Mn binary alloys as a function of Mn content. Open (filled) squares denote μ_0 (m_i) of Fe and open (filled) circles are those of Mn.

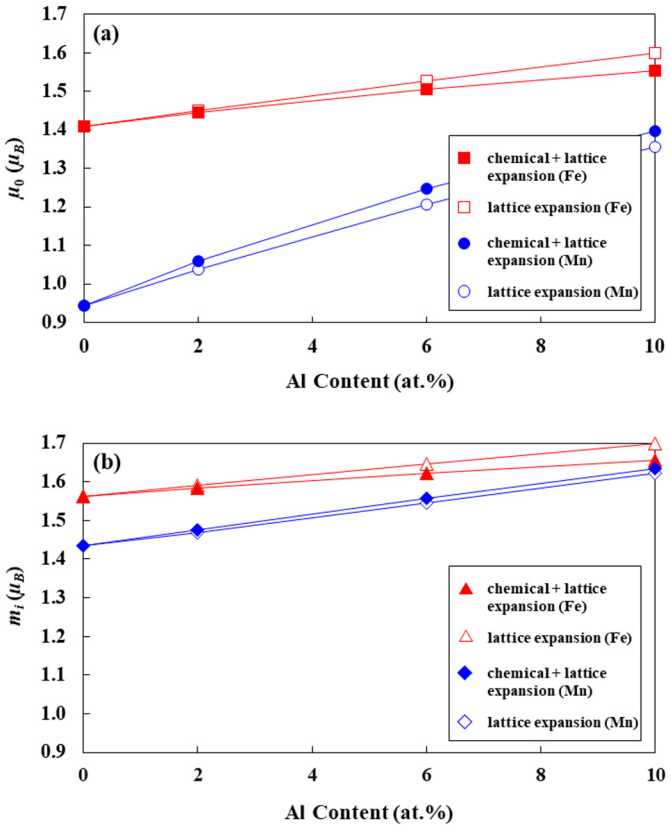

Fig. 2. (a) Static equilibrium local magnetic moment (μ_0) and (b) mean magnetic moment (m_i) of Fe and Mn in the bulk of Fe-20Mn (at.%) alloys with Al addition. The chemical effect by Al marginally changes the magnetic moments from the lattice-expansion-only, both for Fe and Mn.

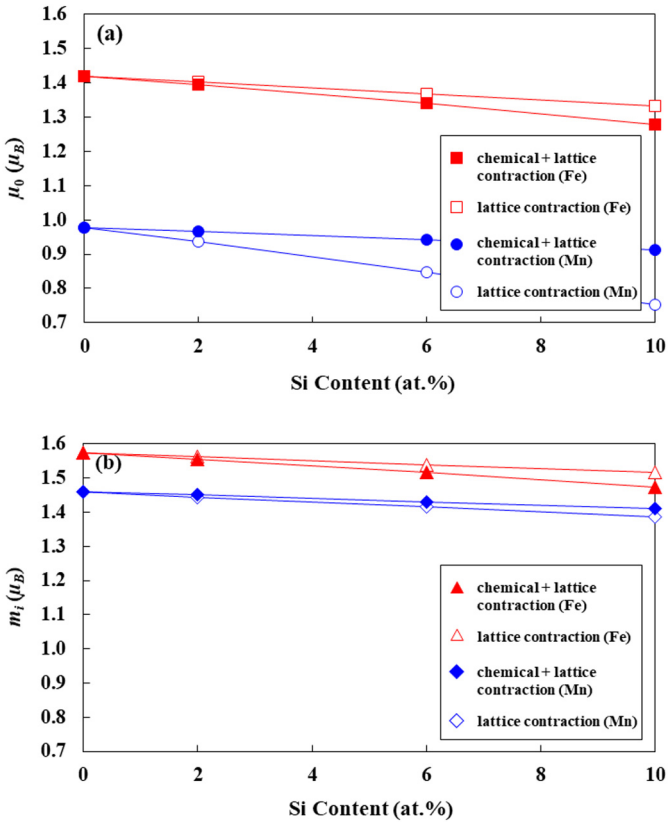

Fig. 3. (a) Static equilibrium local magnetic moment (μ_0) and (b) mean magnetic moment (m_i) of Fe and Mn in the bulk of Fe-30Mn (at.%) alloys with Si addition. Si decreases all the magnetic moments. The chemical and lattice contraction effect by Si on the moments are small compared to those by Al.

the subject of the SFE of Fe-Mn-Al (Si) alloys. In Fig. 4, we show the SFEs of Fe-20Mn (at.%) alloys with Al addition at 298 K. It is found that the SFE decreases with increasing Al content in the FS calculations. The calculated values are γ_{tot} = 128.4, 119.9, 113.0, and 87.9 mJ/m^2 at 0, 2, 6, and 10 at.% Al, respectively. This tendency is contradictory to the experimental observations in which the SFE increases with Al addition [25–27]. On the other hand, we find that the LSFs remedy the deficiency of the FS. The SFE at 0, 2, 6, and 10 at.% Al is calculated to be γ_{tot} = 13.0, 27.2, 41.2, and 48.1 mJ/m^2, respectively. This result agrees well with the experiments [25–30]. It is noteworthy that the LSFs give not only the correct behavior of the SFE with Al alloying but also the reliable SFE values matching perfectly with the experiments as shown in Fig. 4. Allain et al. [15] suggested that Fe-Mn-Al alloys are in the TWIP regime when their SFEs are in the range of 12–35 mJ/m^2, which was confirmed by Jeong et al. [27] with neutron scattering measurements. The LSFs show that Fe-20Mn (at.%) alloys are in the TWIP regime up to 4.5 at.% Al content whereas the FS significantly overestimates the SFE of Fe-Mn-Al alloys out of the TWIP regime.

Next, we show in Fig. 5 the variation of the SFEs of Fe-30Mn (at.%) by Si alloying at 298 K. The FS calculations give that the SFE decreases from 135.8 mJ/m^2 to 73.4 mJ/m^2 as Si content increases from 0 to 10 at.%. This trend is consistent with the experimental observation in which Si decreases the SFE of Fe-Mn alloys [28,33]. However, the theoretical slope of −6 mJ/m^2 per at.% Si in the FS is too large in magnitude compared to that of −1.3 mJ/m^2 per at.% Si in the experiment. It is interesting that the LSFs calculations are in perfect agreement with experiments up to 6 at.% Si addition in Fig. 5 and produce only a small deviation at higher concentration. In the range of 0 to 6 at.% Si, the slope from the LSFs is −2.1 mJ/m^2 per at.% Si, which is very close to the experimental value of −1.3 mJ/m^2 per at.% Si. Because the Si addition in Fe-Mn alloys decreases the SFE, it would be an effective element to induce the TRIP phenomena which is expected with the SFE less than 18 mJ/m^2 [15]. Hence, it is important to note that Si works qualitatively in a very different way from Al.

4. Discussion

Previously, an *ab initio* research examined the influence of Al and Si on the relative stability of the hcp and fcc phase of Fe-Mn alloys [41]. Those results show that Al increases the SFE of Fe-Mn alloys. Our current methodology based on the supercell method also anticipated the

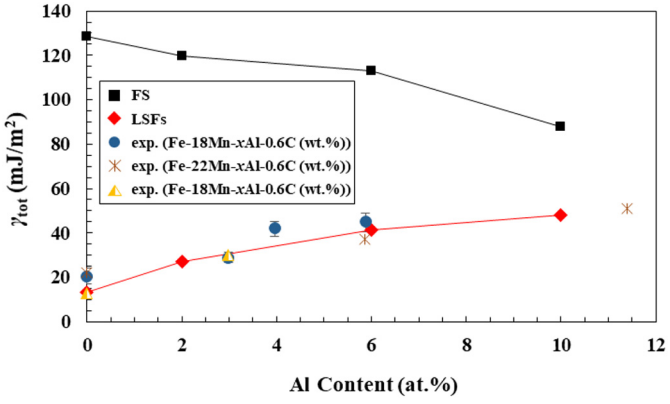

Fig. 4. Effect of Al addition on the SFE (γ_{tot}) of Fe-20Mn (at.%) alloy at 298 K. We employed two computational schemes for the description of the magnetic degrees of freedom: the FS and the LSFs (see the Methods section). γ_{tot} includes both the chemical and lattice expansion effects of Al. Filled circles [27], cross marks [26], and filled triangles [25] represent the experimental values.

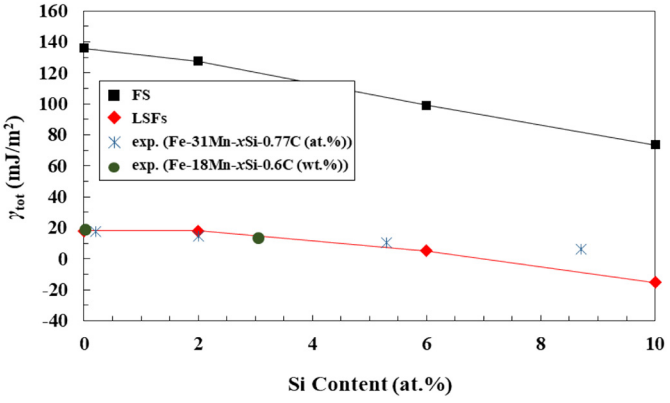

Fig. 5. Effect of Si addition on the SFE (γ_{tot}) of Fe-30Mn (at.%) alloy at 298 K. We employed two computational schemes for the description of the magnetic degrees of freedom: the FS and the LSFs (see the Methods section). γ_{tot} includes both the chemical and lattice contraction effects of Si. Cross marks [33] and filled circles [28] denote the experimental values.

increase of the SFE by Al. However, we would like to emphasize that those previous results were confined to 0 K. When we extend the calculations to 298 K with the same methodology, the slope becomes negative as shown in Fig. 4. The previous results also found that the energy difference $\Delta E = E_{hcp} - E_{fcc}$ is negative, implying that the hcp phase is more stable than the fcc phase. Here, with the LSFs model, we correctly predict both the magnitude and the trend of the SFE upon alloying at 298 K. Therefore, the achievements should be regarded as the complete theoretical development explaining the behavior of SFE of Fe-Mn based alloys.

We would like to mention that the facts that i) the LSFs are connected to the Fe-Mn matrix rather than the alloying elements (Al and Si) and ii) they have a critical influence on the SFE demonstrates a very important aspect: the matrix is crucial in understanding and classifying the alloying effects on the SFE. In other words, it does matter in which host we insert Al and its effect is determined by the complex interaction between the alloying element and the matrix.

In order to understand the effects of the Al and Si additions on the SFE of Fe-Mn alloys, we examine the details of magnetic and volumetric contributions of each alloying element by comparing the results of the two computational schemes, the FS and the LSFs. Fig. 6 is the change of the magnetic moments with Al addition near the stacking fault of Fe-20Mn (at.%) alloy; for a comparison, we also show the change of the bulk values. The FS results in Fig. 6(a) give that the atomic site near the stacking fault has 0.3–0.6 μ_B and 0.8–1.0 μ_B lower magnetic moment for Fe and Mn, respectively, than those of the bulk. On the other hand, in the LSFs calculations, the difference between the magnetic moments near the stacking fault and in the bulk is much smaller compared to the FS. It is less than ~0.2 μ_B for both Fe and Mn independently of the Al content. Considering that the present free energy consists of the internal energy and the –TS term, we can separate the magnetic part γ_{mag} from the SFE as $\gamma_{tot} = \gamma_{int} + \gamma_{mag}$. The large change of the magnetic moment of the stacking fault from the bulk is expected to induce a large γ_{mag} in magnitude. This observation explains why the SFEs in the FS calculations are highly overestimated than those in the LSFs calculations (see Fig. 4). However, as Al is added, the differences of the moments become smaller in the FS calculations; for example, they are $\Delta\mu = 0.66, 0.55, 0.41$ and $0.31\ \mu_B$ for Fe at 0, 2, 6 and 10 at.% Al. Therefore, we find that in the FS, γ_{mag} of Fe-20Mn (at.%) alloys decreases with Al addition and induces a negative slope of γ_{tot} in Fig. 4. On the other hand, because the differences of the moments in the LSFs are small and change little with Al addition γ_{mag} also varies negligibly and does not influence the positive slope of γ_{tot} by the internal energy contribution.

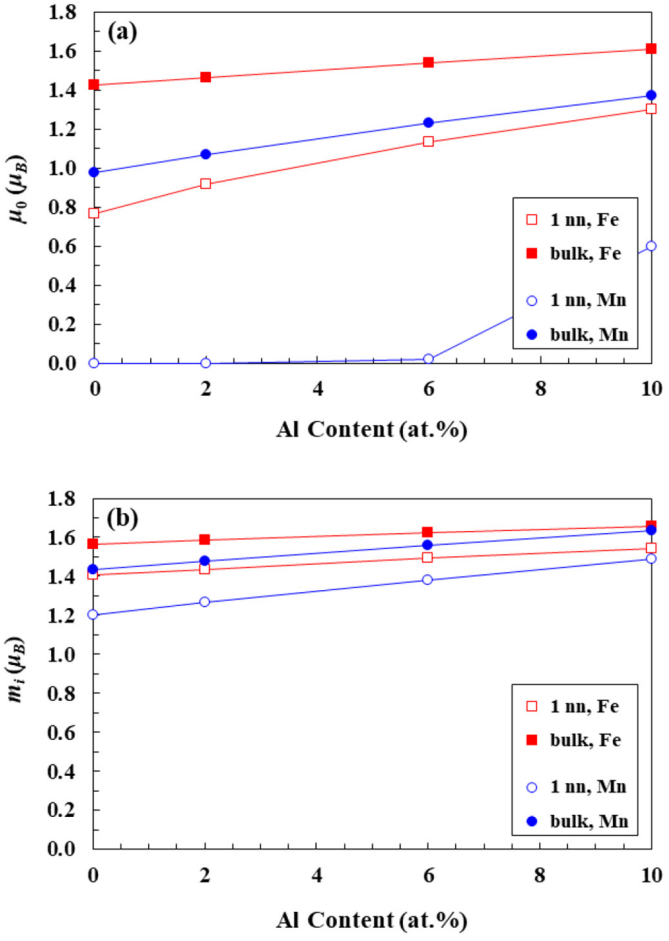

Fig. 6. Effect of Al addition on (a) the static equilibrium magnetic moment (μ_0) and (b) mean magnetic moment (m_i) near the stacking fault and in the bulk of Fe-20Mn (at.%) alloy at 298 K. Both the chemical and lattice expansion effects of Al are included in the data. "1 nn" represents the nearest atomic site to the stacking fault. Open symbols denote the magnetic moments at the 1 nn of the stacking fault and closed symbols are the bulk values.

In Fig. 7, we show the magnetic moment near the stacking fault of Fe-30Mn (at.%) alloy with Si addition. It is found in the FS calculations that the magnetic moment near the stacking fault is reduced by ~0.7 μ_B and ~1.0 μ_B for Fe and Mn, respectively, from those in the bulk. The difference of the magnetic moments near the stacking fault and in the bulk remains almost constant. Therefore, γ_{mag} would not vary much by Si addition. In the LSFs calculations, similarly to the case of Al addition, the difference of the moment is small and also remains constant, which is expected to give a small and uniform contribution to the SFE of Fe-30Mn (at.%) alloys regardless of Si content. With the observations, we would like to emphasize that the change of the SFE of Fe-Mn alloys with Al/Si addition mainly originates from the internal energy part.

The SFEs from the LSFs calculations in Figs. 8 and 9 for Al and Si addition to Fe-Mn alloy, respectively, show that the Al/Si alloying effects can approximately be addressed by considering the volumetric-change-only. For example, the SFE obtained with the expanded volume, which corresponds to the lattice dilation with the Al addition, is in good agreement both with the experiment and the full consideration of chemical effects. With the Al (Si) addition, the slope of the SFE with the lattice expansion only, specifically without chemical alloying, is 3.8 mJ/m^2 per at.% Al (−2.3 mJ/m^2 per at.% Si), which is close to the value considering simultaneously both the chemical effect and lattice expansion effect, 3.5 mJ/m^2 per at.% Al (−3.3 mJ/m^2 per at.% Si). In the FS calculations with Al and Si addition as shown in Figs. 8 and 9, respectively, the volume-induced effects of Al and Si on the internal energy

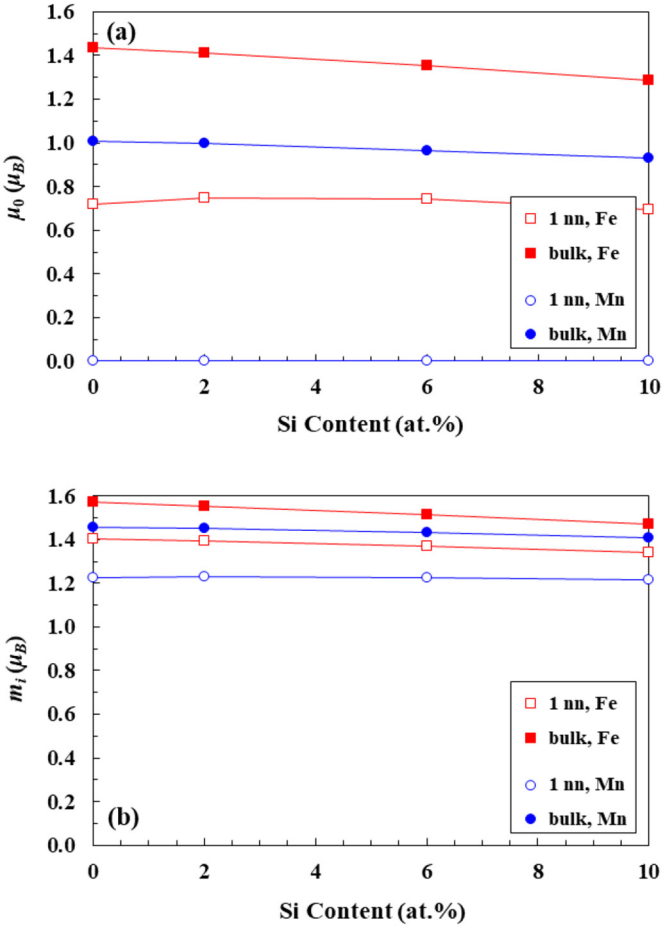

Fig. 7. Effect of Si addition on (a) the static equilibrium magnetic moment (μ_0) and (b) mean magnetic moment (m_i) near the stacking fault and in the bulk of Fe-30Mn (at.%) alloy at 298 K. "1 nn" indicates the nearest atomic layer to the stacking fault. The difference of the magnetic moments near the stacking fault and in the bulk remains almost constant for both the FS (a) and the LSFs (b).

part of the SFE, γ_{int}, seem to reproduce the experimental trends of the alloying effects reasonably well. However, the temperature effects are not considered in this scheme so that this should not be regarded as a complete picture. Meanwhile, the results with the LSFs imply that both Al and Si effects on the SFE of Fe-Mn alloy are dominated by their volumetric effects, which provides the atomic-level mechanisms for the increment and decrement of the SFE by the Al and Si alloying, respectively. We recall that similar mechanisms were proposed for the effects of interstitial alloying elements such as carbon and nitrogen on the SFE of iron-based alloys [34,59].

According to the theory proposed by Lee et al. [59], the volumetric effect on the SFE can be obtained based on a simple physical picture. Let $\gamma(V)$ be the SFE of an fcc lattice at the atomic volume V. Then, we can write the SFE as $\gamma(V) = \gamma(V_0) + \alpha(a - a_0)$ around the equilibrium volume V_0, where a and a_0 are the lattice constants given by $a = (4V)^{1/3}$ and $a_0 = (4V_0)^{1/3}$, respectively. In this expression, the linear coefficient α represents the slope of the SFE against the lattice parameter. One can find $\alpha = 2\sqrt{3}B_h\{(V_0 - V_1)/V_1\}$, where B_h is the bulk modulus of the hexagonal close-packed (hcp) structure and V_1 is the equilibrium volume of the hcp structure. Since in Fe-based alloys the hcp lattice usually has smaller volume than the fcc one (due to the lower magnetic pressure), we can assume a positive value for α. Therefore, the increment of the SFE in Fe-Mn alloys by lattice expansion or the decrease by the lattice contraction can be understood through the above theoretical framework.

Here, we would like to mention how the LSFs are affected by volume change. It is well known that the lattice expansion generally induces an enhanced magnetic moment by electron localization [60–64]. In paramagnetic Fe-Mn alloys, this process can be understood with the local density of states in which electrons in the minority-spin states near the Fermi level E_F are transferred to the majority-spin states. Accordingly, μ_0 increases with the lattice expansion, and the weight of the spin-density distribution $x_i(\mu)$ moves toward the higher moments. The change is reflected by the increase of m_i, as indicated in Fig. 2(b).

Finally, we would like to talk about the influence of interstitial carbon on the SFE of Fe-Mn-Al (Si) alloys. The main role of the interstitial atoms in terms of the SFE will come from the lattice-expansion effect as far as the concentration is low [34,59]. In this sense, disregarding the chemical effect of carbon, we examine the case of 0.6 wt% C addition to Fe-Mn alloys by employing the experimental data for the lattice variation by carbon in Fe-Mn; carbon gives rise to a lattice-expansion coefficient by concentration 0.041 Å/wt% C (or 0.009 Å/at.% C) [19]. Using the corresponding volume, we find that in the LSFs the mean slope of the SFE against the Al content decreases from 3.5 mJ/m^2 per at.% Al without carbon to 1.7 mJ/m^2 per at.% Al with 0.6 wt% C. This can also be checked in Fig. 4 where the increment of the SFE with Al addition goes slower. Meanwhile, in experiments the mean slope of the SFE at 0.15 wt% C content is 5.5 mJ/m^2 per at.% Al [31], which is higher than that of 4.1 mJ/m^2 per at.% Al reported for 0.6 wt% C [25–27]. Although the change of the slope of the SFE by carbon is sizable we notice that the sign of the slope remains positive even by carbon addition. In the case of Si addition, the slope of the SFE with the LSFs changes little

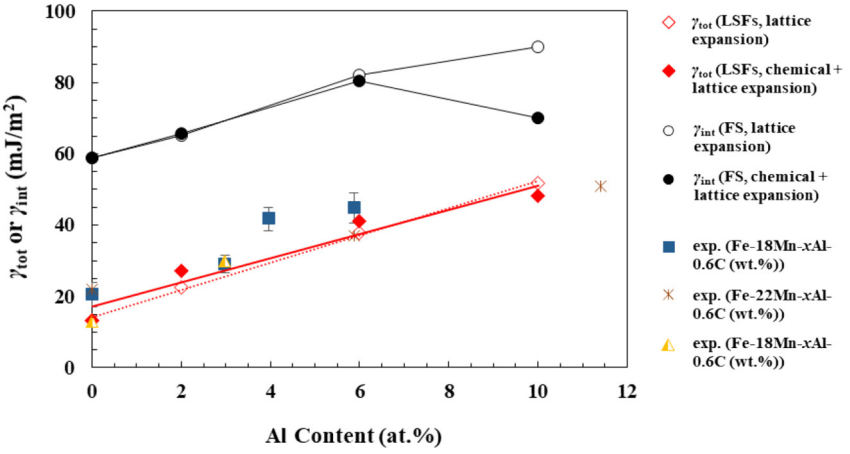

Fig. 8. Volumetric effect of Al on the SFE (γ_{tot}) of Fe-20Mn (at.%) alloy at 298 K. The dotted and solid lines denote a linear regression of the SFEs by the volumetric-effect-only and both the chemical and volumetric effects of Al, respectively, in the LSFs calculations. Open and filled circles are the internal energy part of the SFE (γ_{int}) in the FS calculations.

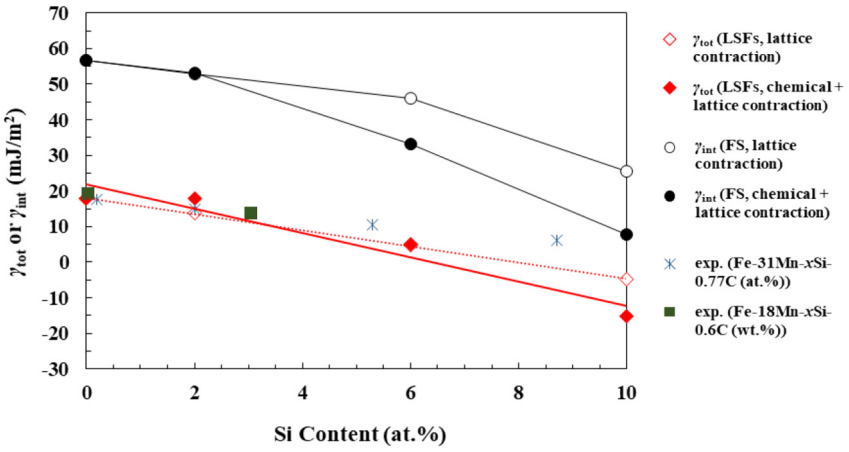

Fig. 9. Volumetric effect of Si addition on the SFE (γ_{tot}) of Fe-30Mn (at.%) alloy at 298 K. The dotted and solid lines are a linear regression of the SFEs by the volumetric-effect-only and both the chemical and volumetric effects of Si, respectively, in the LSFs calculations. Open and filled circles indicate the internal energy part of the SFE (γ_{int}) in the FS calculations.

when we add 0.17 wt% C according to the composition in the experiments [33]. Hence, it is expected that the slope of the SFE by Al and Si will not significantly influenced by the inclusion of carbon.

5. Conclusions

We have investigated the effects of Al or Si addition on the SFE of Fe-Mn alloys by using an *ab initio* method. The LSFs model was introduced in order to describe the paramagnetic state at finite temperature. It was shown that Al addition influences the thermal spin fluctuations mainly through the lattice expansion. On the other hand, Si is less effective to the lattice variation in magnitude and thus does not much affect the magnetic fluctuations compared to Al. The FS calculations predict a decrement of the SFE of Fe-Mn alloys with Al addition, which is contrary to the experimental observations. However, the LSFs remedy the deficiency and give the increment of the SFE in agreement with the experiments. Since both Al and Si are non-magnetic additions, the critical role of the magnetic degree of freedom in the paramagnetic state is quite unexpected and our finding demonstrates the role of the host matrix in the alloying effects on SFE. Finally, we also estimated the carbon effects on the SFE of Fe-Mn-Al (Si) alloys by accounting for the volumetric term, and the experimental C levels are predicted to have moderate effect on the SFE slopes *versus* Al and Si. The present findings underline the importance of the thermal LSFs in the proper description of the SFE of high Mn steels which is indispensable for the efficient design of advanced high-strength steels.

CRediT authorship contribution statement

Young Won Choi: Conceptualization, Investigation, Writing - Original Draft. **Dong Zhihua:** Writing - Review & Editing. **Wei Li:** Software. **Stephan Schönecker:** Writing - Review & Editing. **Hansoo Kim:** Writing - Review & Editing. **Se Kyun Kwon:** Writing - Review & Editing. **Levente Vitos:** Conceptualization, Supervision, Writing - Review & Editing.

Declaration of competing interest

The authors declare that they have no known competing financial interests or personal relationships that could have appeared to influence the work reported in this paper.

Acknowledgements

This work was supported by the Swedish Research Council (2015-5335 and 2017-06474), the Swedish Foundation for Strategic Research (S14-0038 and SM16-0036), the Swedish Foundation for International Cooperation in Research and Higher Education (CH2015-6292), the Basic Science Research Program through the National Research Foundation of Korea (NRF-2017R1A2A1A18071775), the China Scholarship Council, the Hungarian Scientific Research Fund (OTKA 128229), the Carl Trygger Foundation, and the National Natural Science Foundation of China (NSFC, Projects No. 51611130062 and 51374260). The calculations were performed on resources provided by the Swedish National Infrastructure for Computing (SNIC) at the National Supercomputer Centre (NSC) in Linköping.

Data availability

The raw/processed data required to reproduce these findings cannot be shared at this time due to technical or time limitations.

References

[1] B.C. De Cooman, Y. Estrin, S.K. Kim, Twinning-induced plasticity (TWIP) steels, Acta Mater. 142 (2018) 283–362.
[2] B.C. De Cooman, O. Kwon, K.-G. Chin, State-of-the-knowledge on TWIP steel, Mater. Sci. Tech. 28 (2012) 513–527.
[3] B.C. De Cooman, 11 - High Mn TWIP steel and medium Mn steel, in: R. Rana, S.B. Singh (Eds.), Automotive Steels: Design, Metallurgy, Processing and Applications, Woodhead Publishing 2017, pp. 317–385.
[4] S.-J. Lee, J. Han, S. Lee, S.-H. Kang, S.-M. Lee, Y.-K. Lee, Design for Fe-high Mn alloy with an improved combination of strength and ductility, Sci. Rep. 7 (2017) 3573.
[5] P. Chowdhury, D. Canadinc, H. Sehitoglu, On deformation behavior of Fe-Mn based structural alloys, Mater. Sci. Eng. R 122 (2017) 1–28.
[6] O. Grässel, L. Krüger, G. Frommeyer, L.W. Meyer, High strength Fe–Mn–(Al, Si) TRIP/TWIP steels development — properties — application, Int. J. Plast. 16 (2000) 1391–1409.
[7] R. Kalsar, S. Suwas, A novel way to enhance the strength of twinning induced plasticity (TWIP) steels, Scr. Mater. 154 (2018) 207–211.
[8] H.K. Yang, Y.Z. Tian, Z.J. Zhang, Z.F. Zhang, Simultaneously improving the strength and ductility of Fe-22Mn-0.6C twinning-induced plasticity steel via nitrogen addition, Mater. Sci. Eng. A 715 (2018) 276–280.
[9] F. Kies, P. Köhnen, M.B. Wilms, F. Brasche, K.G. Pradeep, A. Schwedt, S. Richter, A. Weisheit, J.H. Schleifenbaum, C. Haase, Design of high-manganese steels for additive manufacturing applications with energy-absorption functionality, Mater. Des. 160 (2018) 1250–1264.
[10] X. Li, L. Chen, Y. Zhao, R.D.K. Misra, Influence of manganese content on ε-/α′- martensitic transformation and tensile properties of low-C high-Mn TRIP steels, Mater. Des. 142 (2018) 190–202.
[11] Z. Guo, L. Li, Influences of alloying elements on warm deformation behavior of high-Mn TRIP steel with martensitic structure, Mater. Des. 89 (2016) 665–675.
[12] G. Frommeyer, U. Brüx, P. Neumann, Supra-ductile and high-strength manganese-TRIP/TWIP steels for high energy absorption purposes, ISIJ Inter. 43 (2003) 438–446.
[13] Z.C. Luo, M.X. Huang, Revisit the role of deformation twins on the work-hardening behaviour of twinning-induced plasticity steels, Scr. Mater. 142 (2018) 28–31.
[14] Z.C. Luo, R.D. Liu, X. Wang, M.X. Huang, The effect of deformation twins on the quasi-cleavage crack propagation in twinning-induced plasticity steels, Acta Mater. 150 (2018) 59–68.

[15] S. Allain, J.-P. Chateau, O. Bouaziz, S. Migot, N. Guelton, Correlations between the calculated stacking fault energy and the plasticity mechanisms in Fe-Mn-C alloys, Mater. Sci. Eng. A 387-389 (2004) 158–162.
[16] D.T. Pierce, J.A. Jiménez, J. Bentley, D. Raabe, J.E. Wittig, The influence of stacking fault energy on the microstructural and strain-hardening evolution of Fe-Mn-Al-Si steels during tensile deformation, Acta Mater. 100 (2015) 178–190.
[17] J.-H. Kang, T. Ingendahl, W. Bleck, A constitutive model for the tensile behaviour of TWIP steels: composition and temperature dependencies, Mater. Des. 90 (2016) 340–349.
[18] D.T. Pierce, J. Bentley, J.A. Jiménez, J.E. Wittig, Stacking fault energy measurements of Fe–Mn–Al–Si austenitic twinning-induced plasticity steels, Scr. Mater. 66 (2012) 753–756.
[19] S.-J. Lee, Y.-S. jung, S.-I. Baik, Y.-W. Kim, M. Kang, W. Woo, Y.-K. Lee, The effect of nitrogen on the stacking fault energy in Fe–15Mn–2Cr–0.6C–xN twinning-induced plasticity steels, Scr. Mater. 92 (2014) 23–26.
[20] S.-J. Lee, K. Ushioda, H. Fujii, Evaluation of stacking-fault energy in Fe-Mn based twinning-induced plasticity steels after friction stir welding, Mater. Char. 147 (2019) 379–383.
[21] O. Zambrano, Stacking fault energy maps of Fe-Mn-Al-C steels: effect of temperature, grain size and variations in compositions, J. Eng. Mater. Tech. 138 (2016), 041010.
[22] R. Xiong, H. Peng, H. Si, W. Zhang, Y. Wen, Thermodynamic calculation of stacking fault energy of the Fe–Mn–Si–C high manganese steels, Mater. Sci. Eng. A 598 (2014) 376–386.
[23] R. Xiong, H. Peng, S. Wang, H. Si, Y. Wen, Effect of stacking fault energy on work hardening behaviors in Fe–Mn–Si–C high manganese steels by varying silicon and carbon contents, Mater. Des. 85 (2015) 707–714.
[24] D.T. Pierce, J.A. Jiménez, J. Bentley, D. Raabe, C. Oskay, J.E. Wittig, The influence of manganese content on the stacking fault and austenite/ε-martensite interfacial energies in Fe–Mn–(Al–Si) steels investigated by experiment and theory, Acta Mater. 68 (2014) 238–253.
[25] J. Kim, S.-J. Lee, B.C. De Cooman, Effect of Al on the stacking fault energy of Fe-18Mn-0.6C twinning-induced plasticity, Scr. Mater. 65 (2011) 363–366.
[26] K.-T. Park, K.G. Jin, S.H. Han, S.W. Hwang, K. Choi, C.S. Lee, Stacking fault energy and plastic deformation of fully austenitic high manganese steels: effect of Al addition, Mater. Sci. Eng. A 527 (2010) 3651–3661.
[27] J.S. Jeong, W. Woo, K.H. Oh, S.K. Kwon, Y.M. Koo, In situ neutron diffraction study of the microstructure and tensile deformation behavior in Al-added high manganese austenitic steels, Acta Mater. 60 (2012) 2290–2299.
[28] K. Jeong, J.-E. Jin, Y.-S. Jung, S. Kang, Y.-K. Lee, The effects of Si on the mechanical twinning and strain hardening of Fe-18Mn-0.6C twinning-induced plasticity steel, Acta Mater. 61 (2013) 3399–3410.
[29] J.-E. Jin, Y.-K. Lee, Effects of Al on microstructure and tensile properties of C-bearing high Mn TWIP steel, Acta Mater. 60 (2012) 1680–1688.
[30] M. Kang, W. Woo, Y.-K. Lee, B.-S. Seong, Neutron diffraction analysis of stacking fault energy in Fe-18Mn-2Al-0.6C twinning-induced plasticity steels, Mater. Lett. 76 (2012) 93–95.
[31] X. Tian, H. Li, Y. Zhang, Effect of Al content on stacking fault energy in austenitic Fe-Mn-Al-C alloys, J. Mater. Sci. 43 (2008) 6214–6222.
[32] H.K. Yang, Y.Z. Tian, Z.F. Zhang, Revealing the mechanical properties and microstructure evolutions of Fe–22Mn–0.6C–(x)Al TWIP steels via Al alloying control, Mater. Sci. Eng. A 731 (2018) 61–70.
[33] X. Tian, Y. Zhang, Effect of Si content on the stacking fault energy in γ-Fe-Mn-Si-C alloys: part I. X-ray diffraction line profile analysis, Mater. Sci. Eng. A 516 (2009) 73–77.
[34] S. Lu, R. Li, K. Kádas, H. Zhang, Y. Tian, S.K. Kwon, K. Kokko, Q.-M. Hu, S. Hertzman, L. Vitos, Stacking fault energy of C-alloyed steels: the effect of magnetism, Acta Mater. 122 (2017) 72–81.
[35] W. Li, S. Lu, D. Kim, K. Kokko, S. Hertzman, S.K. Kwon, L. Vitos, First-principles prediction of the deformation modes in austenitic Fe-Cr-Ni alloys, Appl. Phys. Lett. 108 (2016), 081903.
[36] S. Huang, W. Li, S. Lu, F. Tian, J. Shen, E. Holmström, L. Vitos, Temperature dependent stacking fault energy of FeCrCoNiMn high entropy alloy, Scr. Mater. 108 (2015) 44–47.
[37] S. Lu, Q.-M. Hu, B. Johansson, L. Vitos, Stacking fault energies of Mn, co and Nb alloyed austenitic stainless steels, Acta Mater. 59 (2011) 5728–5734.
[38] L. Vitos, P.A. Korzhavyi, B. Johansson, Evidence of large magnetostructural effects in austenitic stainless steels, Phys. Rev. Lett. 96 (2006), 117210.
[39] L. Vitos, J.-O. Nilsson, B. Johansson, Alloying effects on the stacking fault energy in austeniteic stainless steels from first-principles theory, Acta Mater. 54 (2006) 3821–3826.
[40] Z. Dong, S. Schönecker, D. Chen, W. Li, S. Lu, L. Vitos, Influence of Mn content on the intrinsic energy barriers of paramagnetic FeMn alloys from longitudinal spin fluctuation theory, Int. J. Plast. 119 (2019) 123–139.
[41] T. Gebhardt, D. Music, M. Ekholm, I.A. Abrikosov, L. Vitos, A. Dick, T. Hickel, J. Neugebauer, J.M. Schneider, The influence of additions of Al and Si on the lattice stability of fcc and hcp Fe-Mn random alloys, J. Phys. Condens. Matter 23 (2011), 246003.
[42] J. Nakano, P.J. Jacques, Effects of the thermodynamic parameters of the hcp phase on the stacking fault energy calculations in the Fe-Mn and Fe-Mn-C systems, CALPHAD: Comp. Coup. Phase Diag. Thermochem. 34 (2010) 167–175.
[43] A. Dumay, J.-P. Chateau, S. Allain, S. Migot, O. Bouaziz, Influence of addition elements on the stacking-fault energy and mechanical properties of an austenitic Fe-Mn-C steel, Mater. Sci. Eng. A 483-484 (2008) 184–187.
[44] A.J. Pindor, J. Staunton, G.M. Stocks, H. Winter, Disordered local moment state of magnetic transition metals: a self-consistent KKR CPA calculation, J. Phys. F: Met. Phys. 13 (1983) 979–989.
[45] J. Staunton, B.L. Gyorffy, A.J. Pindor, G.M. Stocks, H. Winter, The "disordered local moment" picture of itinerant magnetism at finite temperatures, J. Magn. Magn. Mater. 45 (1984) 15–22.
[46] P. Hohenberg, W. Kohn, Inhomogeneous electron gas, Phys. Rev. 136 (1964) B864–B871.
[47] W. Kohn, L.J. Sham, Self-consistent equations including exchange and correlation effects, Phys. Rev. 140 (1965) A1133–A1138.
[48] L. Vitos, Total-energy method based on the exact muffin-tin orbitals theory, Phys. Rev. B 64 (2001), 014107.
[49] J.P. Perdew, W. Yue, Accurate and simple density functional for the electronic exchange energy: generalized gradient approximation, Phys. Rev. B 33 (1986) 8800–8802.
[50] J.P. Perdew, K. Burke, M. Ernzerhof, Generalized gradient approximation made simple, Phys. Rev. Lett. 77 (1996) 3865–3868.
[51] P. Soven, Coherent-potential model of substitutional disordered alloys, Phys. Rev. 156 (1967) 809–813.
[52] B.L. Gyorffy, Coherent-potential approximation for a nonoverlapping-muffin-tin-potential model of random substitutional alloys, Phys. Rev. B 5 (1972) 2382–2384.
[53] Z. Dong, S. Schönecker, D. Chen, W. Li, M. Long, L. Vitos, Elastic properties of paramagnetic austenitic steel at finite temperature: longitudinal spin fluctuations in multicomponent alloys, Phys. Rev. B 96 (2017), 174415.
[54] Z. Dong, W. Li, S. Schönecker, S. Lu, D. Chen, L. Vitos, Thermal spin fluctuation effect on the elastic constants of paramagnetic Fe from first principles, Phys. Rev. B 92 (2015), 224420.
[55] Z. Dong, W. Li, D. Chen, S. Schönecker, M. Long, L. Vitos, Longitudinal spin fluctuation contribution to thermal lattice expansion of paramagnetic Fe, Phys. Rev. B 95 (2017), 054426.
[56] C.-M. Li, F. Sommer, E.J. Mittemeijer, Characteristics of the γ→α transformation in Fe-Mn alloys, Mater. Sci. Eng. A 325 (2002) 307–319.
[58] X. Lu, Z. Qin, X. Tian, Y. Zhang, B. Ding, Z. Hu, Relations between the lattice parameter and the stability of austenite against ε martensite for the Fe-Mn based alloys, J. Mater. Sci. Tech. 19 (2003) 443–446.
[59] J.-Y. Lee, Y.M. Koo, S. Lu, L. Vitos, S.K. Kwon, The behaviour of stacking fault energy upon interstitial alloying, Sci. Rep. 7 (2017) 11074.
[60] D. Bagayoko, J. Callaway, Lattice-parameter dependence of ferromagnetism in bcc and fcc iron, Phys. Rev. B 28 (1983) 5419–5422.
[61] G. Fuster, N.E. Brener, J. Callaway, J.L. Fry, Y.Z. Zhao, D.A. Papaconstantopoulos, Magnetism in bcc and fcc manganese, Phys. Rev. B 38 (1988) 423–432.
[62] C. Jing, S.X. Cao, J.C. Zhang, Lattice constant dependence of magnetic properties in bcc and fcc Fe_xMn_{1-x} alloys, Phys. Rev. B 68 (2003), 224407.
[63] H.L. Zhang, S. Lu, M.P.J. Punkkinen, Q.-M. Hu, B. Johansson, L. Vitos, Static equation of state of bcc iron, Phys. Rev. B 82 (2010), 132409.
[64] H. Zhang, B. Johansson, L. Vitos, Density-functional study of paramagnetic iron, Phys. Rev. B 84 (2011), 140411.
[65] I.-C. Jung, B.C. De Cooman, Temperature dependence of the flow stress of Fe-18Mn-0.6C-xAl twinning-induced plasticity steel, Acta Mater. 61 (2013) 6724–6735.